CHAPTER 3

Integrated zero-order fuzzy-controlled shape optimization

3.1 Introduction

Structural shape optimization is a process of designing structures that are both functional and efficient. It focuses on a way to improve the overall shape of the structure within the sense that it satisfies the given constraints imposed on it. The goal of the process is to find the optimal shape of a structure that satisfies the required performance criteria while minimizing material usage and cost. This is achieved by using mathematical optimization techniques that take into account the behaviour of the structure under different loading conditions. As discussed in previous chapters there are two main approaches to structural shape optimization: gradientless methods/non-gradient methods/zero-order methods and gradient-based methods. The present study proposes a method for structural shape optimization using fuzzy membership functions that integrates multiple criteria and utilizes a zero-order approach. The method incorporates automated mesh construction, refinement at each iteration, and the use of design elements to create a smooth shape and remove undesirable jagged edges. The previous methods used so far in industries are unable to remove sharp corners and jagged edges, causing too many regions of stress concentration. These have been

addressed and taken care of in the currently suggested approach. The mobility of design nodes as well as the ultimate convergence is controlled using fuzzy set theory. The proposed approach is based upon the notion of non-gradient shape optimization and packaged in a piece of software termed GSO (Gradientless shape optimization) coded in the FORTRAN language. The current approach attempts to establish the efficiency of non-gradient methods and prove their competence in the field of shape optimization. A few examples have been worked upon to show the efficiency of the approach using different constraints like initial imperfections, fixed beams with different materials, beams with different types of loadings, and beams with flat tops. The approach seems to work in all conditions properly and gives a successfully optimized shape of different structures. To understand the whole process of shape optimization using GSO lets discuss its overall working procedure in detail but before that one should have some basic understanding of fuzzy logic.

3.2 Fuzzy logic

Fuzzy logic was first developed by Lofti A. Zadeh in the year 1965. The purpose of its development was to induce a grossly oversimplified way of real-world challenges in the mathematical world. It exploits the degrees of truthiness or falseness of any statement instead of the usual 0 or 1 like Boolean logic. The belongingness of an element to a fuzzy set can not only be stated using 0 and 1, but also by any value ranging from 0 to 1 signifying the element's degree of membership to that set. This can be explained using Figure 3.1.

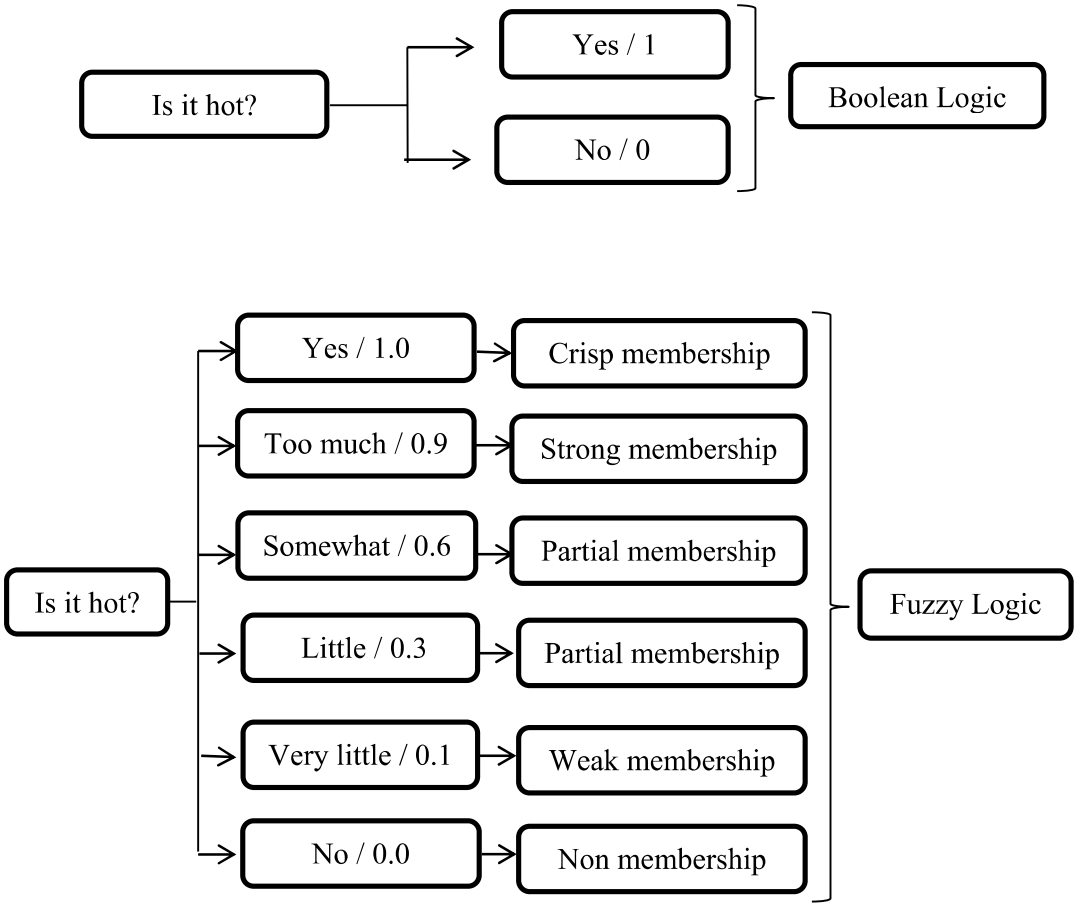

Figure 3.1: Degree of membership.

Hence, fuzzy logic is not itself fuzzy in nature instead it describes the fuzziness of anything. Assuming 'X' as the universal set having elements denoted by 'x'. Subset A then can be called a fuzzy set when the valuation set is in the real interval [0,1]. It can be characterized by Equation 3.1

$$A = \{(x, \mu_a(x)), x \in X\} \tag{3.1}$$

Where, $\mu_a(X)$ is the membership grade of 'x' in 'A'. The more closely 'x' corresponds to 'A'; the closer its value is near 1. Both non-linear and linear membership functions are possible for a fuzzy set.

3.2.1 Fuzzy Intersections

The fuzzy intersection of the sets can be defined using Equation 3.2. It follows when two fuzzy sets A and B with associated supports for membership A(x) and B(x) are supplied.

$$\mu_{A\cup B}(x) = \mu_A(x) \cap \mu_B(x)$$
$$= \min \{\mu_A(x), \mu_B(x) \tag{3.2}$$

3.2.2 Fuzzy Unions

The fuzzy unions of the sets can be defined using Equation 3.3. It follows when two fuzzy sets A and B with associated supports for membership A(x) and B(x) are supplied.

$$\mu_{A\cup B}(x) = \mu_A(x) \cup \mu_B(x)$$
$$= \max \{\mu_A(x), \mu_B(x) \tag{3.3}$$

3.2.3 Fuzzy Differences / Compliments

The fuzzy difference or compliment associated to $\mu_A(x)$ can be given by Equation 3.4

$$\mu_{\bar{A}}(x) = 1 - \mu_A(x) \tag{3.4}$$

Figure 3.2 illustrates the fuzzy set operations of union, intersection, and complement respectively.

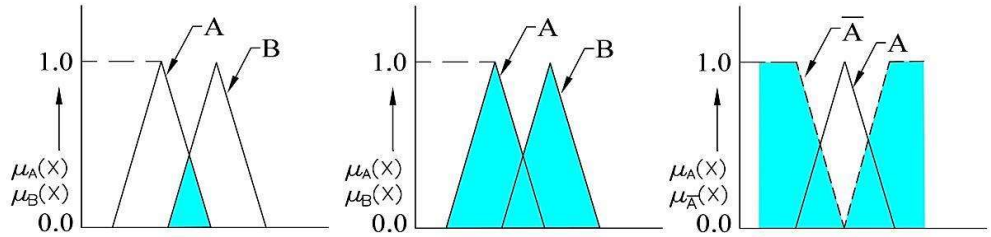

(a) (b) (c)

Figure 3.2: Fuzzy set operations: (a) Intersection, (b) Union, and (c) Complement

One can consult Zimmermann (1996) book for further information on fuzzy set theory.

3.3 Integrated Zero-order method

The zero-order method taken up in previous literatures (Jose, 1990; Sibal, 1992) for structural shape optimization considered the nodes present at the boundary as design variables. These nodal co-ordinates were changed based on the results of the finite element analysis. Finite element meshes are updated after a certain number of iterations to control mesh distortion. There are two significant downsides to this kind of zero-order method.

1. Since boundary node co-ordinates are used as design variables without taking boundary smoothness into account, this may result in sharp edges and an undesirable shape.
2. The optimization procedure may take a long time since manual mesh refining must be done after a certain number of iterations.

To overcome these difficulties in the present study, an automatic mesh generator and refiner have been created with an integrated zero-order method for model generation and optimization. The main focus of the approach is on optimization efficiency and its adaptability to different initial complexities. It aims to represent the model's boundary geometry in a convenient way using design elements and design nodes. The approach also includes automatic mesh generation and re-meshing of the model at every iteration. The convergence and nodal movement are controlled using fuzzy membership theory.

3.3.1 Finite element modelling

Finite element modelling has a significant impact on how accurate the outcomes of shape optimization are. “Also the finite element modelling is by no means unique, and the success of the analysis depends not only on our computational resources but even

more on the way we use them, i.e. what element and what nodal positions we choose," argues P. Pederson, one of the pioneers in structural optimization.

Choosing the right design variable is essential for getting the best shape. However, a direct linkage between the actual geometry and the design variables' values is also essential. In the early years of shape optimization, the boundary nodes co-ordinates were employed as design variables; however, this led to an increased number of design variables and it frequently produced impractical shapes for the final design. Polynomials with coefficients were chosen by a few researchers as design variables to describe the shape. However, the main issue with employing higher-order polynomials is that they might produce an oscillating boundary shape. The next step was to use Bezier and B-spline curves to represent the shape and later the design element idea is also used. In Chapter 2 of the present study, the application of design elements Imam, (1982) and Braibant and Flury, (1984) in shape optimization is discussed.

3.3.2 Model generation

To ensure the accuracy of the finite element model during shape optimization, it is essential to generate a new mesh at each iteration to accommodate changes to the boundary shape. The new mesh is necessary due to changes in geometric and loading conditions and the resulting distortion of elements, which the previous mesh cannot account for. The isoparametric mapping technique is employed along with the design element concept to ensure that the design variable controlling the finite element mesh is also controlling the optimization model, thereby meeting the aforementioned criteria.

The proposed methodology for optimization of structures involves partitioning the structure into a required number of design elements, and each of these elements is defined by a set of keynodes called master nodes, which control the design element's

geometry. The design elements are then divided into smaller finite elements with the help of these master nodes. Figure 3.3 shows the different stages of the discretization of the beam.

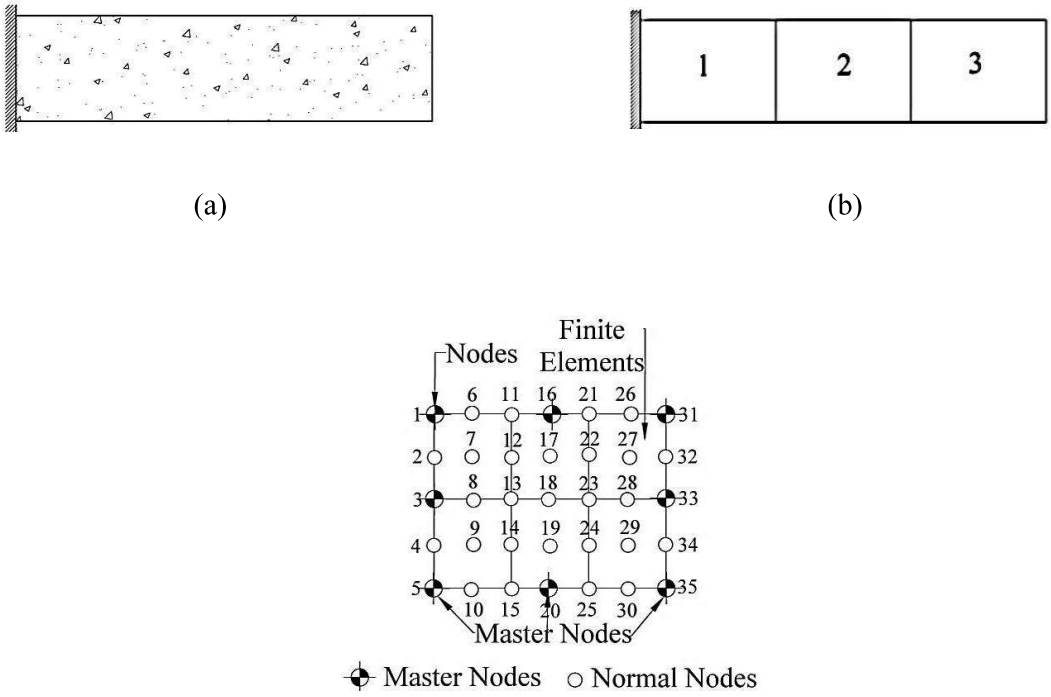

Figure 3.3 (a) Cantilever beam, (b) Division of the model into design elements 1, 2, and 3, (c) Sub-division of design element no. 1 into finite elements.

The methodology employs a two-dimensional isoparametric interpolation function to define the shape of the design elements. Each design element has eight master nodes, and the master nodes at the boundaries relevant to optimization are designated as design nodes. The design nodes are characterized by their respective co-ordinates, which serve as design variables. Isoparametric mapping is utilized to determine the co-ordinates of the nodal points generated. Considering *'X'* and *'Y'* as co-ordinates for the generated nodal point, it is represented by Equation 3.5:

$$\left.\begin{aligned} X &= \sum_{i=1}^{N_m} N_i(\xi,\eta)\ \cdot X_i \\ Y &= \sum_{i=1}^{N_m} N_i(\xi,\eta)\ \cdot Y_i \end{aligned}\right\} \tag{3.5}$$

Where, X_i and Y_i represent the co-ordinates of the master node *'i'*, ξ and η represents the natural co-ordinates in accordance to the point *(X, Y)*, N_i represents the shape function, N_m represents the number of master nodes present in that design element. From the above relation, it can be inferred that the master nodes control the generated finite element mesh, and hence the geometry changes according to the changed co-ordinates of those master nodes. The optimizer gives the modified co-ordinates of master nodes which at each iteration are sent to the mesh generator for generation of new mesh, to be used by the finite element program. This is how the boundary smoothness is kept in check during optimization.

The use of lower-order elements can give erratic results when dealing with stress concentration problems. Hence, the use of quadratic displacement components offers a nice balance between ease of use and correctness of results. Following this in the present study use of nine noded Lagrangian elements is done for finite element modelling.

3.3.3 Nine-noded lagrangian element

The 9-noded Lagrangian element is a type of finite element used in the field of computational mechanics to model the behaviour of solid materials. This element is particularly useful for simulating the behaviour of materials that exhibit large deformations, such as those found in the civil, aerospace, automotive, and biomedical industries. The 9-noded Lagrangian element is characterized by set of nine nodes, each of them represents a point in space where the material is assumed to be located. These

nodes are connected by a set of eight linear shape functions, which describe the displacement of the material at each node. The element's shape and size can be defined by the position of these nodes and the values of the shape functions. One of the key advantages of the 9-noded Lagrangian element is its ability to accurately capture the large deformations that occur in many materials. This is achieved through the use of a Lagrangian formulation, which is based on the material's reference configuration, rather than its current configuration. This allows the element to accurately represent the deformation of the material, even when large strains and rotations are present. The 9-noded Lagrangian element can also handle different types of boundary conditions, such as displacement and traction, which are commonly used in engineering problems. This element can be used to simulate the behaviour of materials under various loading conditions, including static, dynamic and transient. The illustration in Figure 3.4 shows a second-order rectangular element that belongs to the Lagrangian family. As previously stated, each element has nine nodes, with the first eight nodes being the boundary nodes and the last node being an internal node.

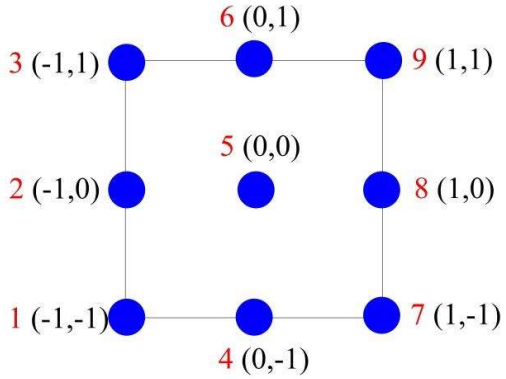

Figure 3.4: Nine-noded lagrangian element.

Elements that belong to the "Lagrange family" are characterized by shape functions that are created by combining the shape functions of one-dimensional

elements. The shape function of the 9-noded lagrangian element is presented in Table 3.1.

Table 3.1: Shape function of the Nine-noded lagrangian element.

Shape Functions	Equation
N_1	$\frac{1}{4}\xi(1-\xi)\eta(1-\eta)$
N_2	$-\frac{1}{4}\xi(1+\xi)\eta(1-\eta)$
N_3	$\frac{1}{4}\xi(1+\xi)\eta(1+\eta)$
N_4	$-\frac{1}{4}\xi(1-\xi)\eta(1+\eta)$
N_5	$-\frac{1}{2}(1-\xi)(1+\xi)\eta(1-\eta)$
N_6	$\frac{1}{2}\xi(1+\xi)(1-\eta)(1+\eta)$
N_7	$\frac{1}{2}(1-\xi)(1+\xi)\eta(1+\eta)$
N_8	$-\frac{1}{2}\xi(1-\xi)(1-\eta)(1+\eta)$
N_9	$(1-\xi^2)(1-\eta^2)$

3.3.4 Fuzzy membership function

The gradientless method for shape optimization involves modifying the geometry in each iteration based on the stress value at the design nodes in the previous iteration. The goal is to achieve a state of full stress where the stress value at each design node is close to the target stress value. However, this is a difficult, as it is imprecise and approximate. To address this issue, fuzzy set theory is used to control the movement of the design nodes and achieve the desired stress value. The approach involves using fuzzy membership functions to find the optimal shape that is closest to the target stress value. Two common shapes of membership functions are used in the fuzzy set theory: bell-shaped and triangular-shaped. The membership value is 1 if the current stress equals the

target stress. Otherwise, it changes in a linear or non-linear manner depending on the type of function used. Below are shown the membership variations for both functions.

a) Bell shaped membership function

The bell shaped membership function exhibits a non-linear membership between the membership value (μ) and the target maximum shear stress (σ_t) as illustrated in Figure 3.5. A mathematical representation of one such curve is given in Equation 3.6.

$$\mu(\sigma) = \frac{1}{(1+(\sigma-\sigma_t)^4)} \tag{3.6}$$

Where, 'σ' represents the design nodes stress value and 'σ_t' represents the target maximum shear stress.

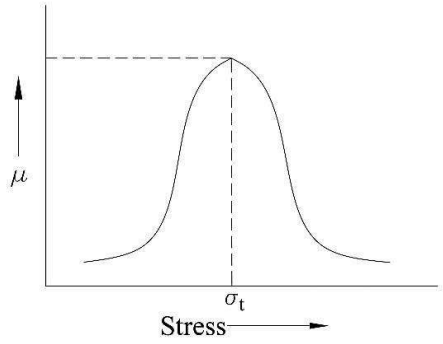

Figure 3.5 Bell shape function

b) Triangular shape membership function

In a triangular shape membership function, a linear relationship is obtained between the membership value (μ) and the target maximum shear stress (σ_t). The value of μ becomes equal to 1 if the design node's stress value (σ) is equal to σ_t as shown in Figure 3.6. It can be expressed mathematically by Equation 3.7:

$$\mu(\sigma) = \begin{cases} \frac{\sigma}{\sigma_t} & if \sigma < \sigma_t \\ 1 & if\ \sigma = \sigma_t \\ 2 - \frac{\sigma}{\sigma_t} & if\ \sigma_t < \sigma < 2\sigma_t \\ 0 & if\ \sigma > 2\sigma_t \end{cases} \quad (3.7)$$

Where, 'σ_t' represents the target maximum shear stress and 'σ' represents the design nodes' stress value.

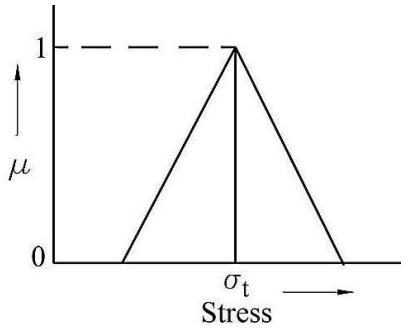

Figure 3.6: Triangular function

For the optimization process to be successful, it is essential to choose the correct membership functions, among the bell or triangle shapes. It is evident from Figure 3.5 that the bell-shaped function's move factor (MF) is larger than the triangle function's, with the exception of areas close to the optimum. The bell-shaped function has non-linear nodal movement, whereas the triangular function has linear nodal movement. The bell function can produce an undesired shape whereas, triangular function convergence may be slow as we approach towards the optimal shape. This is because gradual movement is required when the optimal shape is reached. Hence, a mixed technique, in which the initial iterations are taken up using the bell function and subsequently switching to the triangular function, would be a preferable option. In the present work, a triangular-shaped membership function is utilized due to the reliability and simplicity it possesses.

The material is added when σ is higher than σt, and subtracted when it's lower than σ_t in each iteration, until the design node stress and target stress values are roughly equal. This method uses a fuzzy membership concept that considers the ith node movement to be proportional to the move factor (MF). In the current investigation, the allowable difference between the design node stress and target stress values is 5 N/mm^2 or less. The MF is expressed by Equation 3.8:

$$\left.\begin{array}{ll} \text{If, } \sigma_i > \sigma_t & \text{MF} = \{\mu\ (\sigma_i) - 1\} \\ \text{If, } \sigma_i < \sigma_t & \text{MF} = \{1 - \mu\ (\sigma_i)\} \end{array}\right\} \quad (3.8)$$

The MF versus stress plot for the triangular shape membership function and bell-shaped membership function is shown in Figure 3.7:

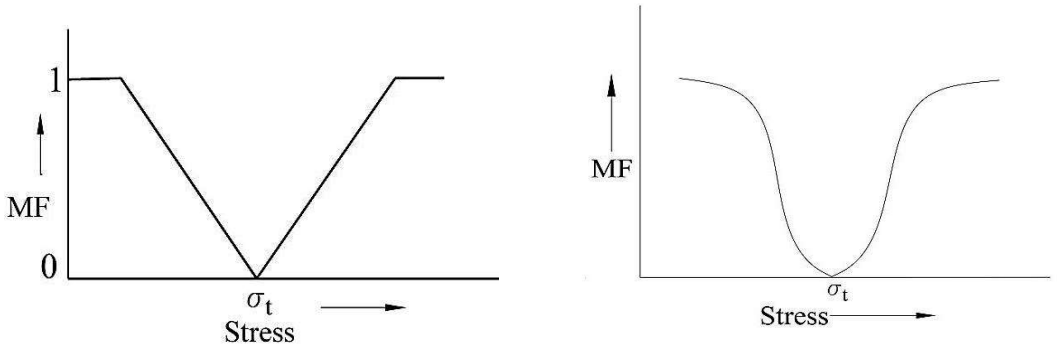

Figure 3.7: Move factor

Figure 3.8 shows the direction of the movement of the design nodes. Here node '*j*' which is the middle node of Lagrangian elements is selected as the direction nodes. The node '*i*' which represents the design node, moves in accordance with the node '*j*'. The smallest distance among all the distances between the design node and their respective direction node is represented by L_{min} which can be expressed mathematically by Equation 3.9:

$$L_{min} = \min_{i=1}^{N_d} (L_i) \tag{3.9}$$

Where, N_d represents the number of design nodes

And $L_i = \sqrt{(X_i - X_j)^2 + (Y_i - Y_j)^2}$

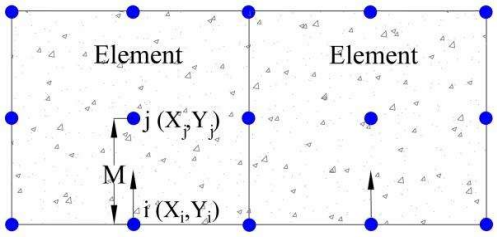

Figure 3.8: Nine noded lagrangian elements with design node 'i' and direction node 'j'

The nodal movement of nodes in the study has been allowed as one-fourth of the full-length movement of L_{min}. Therefore, the movement of design nodes is represented by Equation 3.10:

$$\text{MV}(i) = 0.25 \cdot L_{min} \cdot \text{MF} \tag{3.10}$$

At each iteration, the co-ordinates of the design node 'i' change. This change in co-ordinate can be represented by Equation 3.11:

$$\left.\begin{aligned} X_i' &= X_i + (X_j - X_i) \cdot \frac{MV(i)}{L_i} \\ Y_i' &= Y_i + (Y_j - Y_i) \cdot \frac{MV(i)}{L_i} \end{aligned}\right\} \tag{3.11}$$

Where, X_i' and Y_i' are the newly obtained co-ordinate, and (X_i, Y_i) and (X_j, Y_j) are the co-ordinates for the direction node.

Once a new co-ordinate value is calculated, the optimizer data is retrieved and forwarded to the mesh generator, which creates a new mesh for additional stress analysis. This sequence is repeated iteratively until the convergence criterion is met.

3.3.5 Convergence criteria

The membership function value should always be 1 in ideal circumstances, but because the system is fuzzy, it is challenging for this requirement to be met. As a result, to achieve convergence, the concept of fuzzy interaction or minimum membership function (MMF) has been introduced. The MMF value is adjusted after each iteration and reaches its maximum value for the optimal shape. Therefore, if the MMF value decreases in each iteration and continues to decrease for three consecutive iterations, the program execution stops, and the convergence criteria are considered to be met. It can be mathematically composed of Equation 3.12:

$$\mu(\sigma_{iter}) = \min_{i=1}^{N_d}(\cap \mu\ (\sigma_i)) \tag{3.12}$$

If, $\mu\ (\sigma_{iter}) < \mu\ (\sigma_{iter} + 1)$ continue optimization.

If, $\mu\ (\sigma_{iter}) > \mu\ (\sigma_{iter} + 1)$ cease optimization as convergence has been attained.

3.4 Problem formulation

The present study takes into account a fully stressed design, with stress being optimized at the design nodes. The concrete as presented in section 3.3.2, is modelled as a discretized continuum using nine-noded lagrangian element. The structural elements are analysed using finite element analysis (FEA). Since the process focuses on achieving a fully stressed design, the objective function to be minimized or maximized is stress σ_i at the design nodes such that it becomes more or less equal to σ_t with a tolerance of up to

5 N/mm^2. The value of σ_t can be changed as per the requirement of the user. To fulfil this objective, the design variable selected is design-node/s of concrete which will move to change the shape as explained in section 3.3.4. Another restriction on the permitted amount of deflection (δ) is also provided to ensure that the optimized shape has a regulated deflection. The convergence is achieved using the formulation as explained in section 3.3.5. The overall optimization problem for the present study can be formulated mathematically using Equation 3.13.

Minimize/Maximize $\quad \sigma_i \ (\forall \ \mathrm{i} = 1 \text{ to } \mathrm{n})$ (3.13)

Such that $\begin{cases} \sigma_i \approx \sigma_t \pm 5 \text{ N/mm}^2 \ (\sigma_t \text{ can be decided as per the user requirements}) \\ \text{Deflection } (\delta) \leq \text{Minimum } (Span/250, 20 \text{ mm}) \end{cases}$

Where n is the total number of design nodes.

3.5 Software GSO

A FORTRAN programme titled GSO was created by the author to perform shape optimization using an integrated zero-order technique. Employing nine node Lagrangian plane stress elements, the application performs finite element analysis. In this software, there are twelve primary subroutines. Microsoft Fortran PowerStation 4 has been used to successfully run this programme on AMD Ryzen 5. Below are short summaries of the key subroutines.

a) **Subroutine INPUT:** The majority of the input data, like the number of design elements and their nodal co-ordinates, the properties of the material, the nature of discretization, the support condition, the number of design variables with their directional co-ordinates, etc. are read by this subroutine. Finite element mesh is automatically generated using this data.

b) **Subroutine LOADPS:** The loading data are read by this subroutine. It can support three different kinds of loads viz.: (1) Point load/s (2) Edge weight and (3). Load due to gravity. These are used to calculate the nodal force vector of finite elements.

c) **Subroutine STIFFP:** This subroutine computes each element's stiffness matrix using the Gaussian integration algorithm and stores the results in a disc file.

d) **Subroutine ASSEMBL:** This subroutine puts together a global nodal load vector and global stiffness matrix from the nodal load vector and stiffness matrix of each element.

e) **Subroutine GREDUC:** This subroutine uses the Gaussian reduction approach to carry out the equation elimination procedure for their solution.

f) **Subroutine BACKSUB:** This subroutine's goal is to carry out the back substitution procedure needed after the equation is eliminated using the Gaussian reduction method.

g) **Subroutine DISPLAC:** This subroutine computes the displacements and reactions at the nodes of the finite element.

h) **Subroutine GPSTRESS:** This subroutine computes the stresses at each element's Gauss points, which are then utilised to determine the nodal stresses using appropriate smoothening methods.

i) **Subroutine SHAPE:** This subroutine uses an integrated zero-order technique to perform the shape optimization. Stress smoothening uses fuzzy set theory.

j) **Subroutine RMESH:** This subroutine updates the finite element mesh according to the updated design node co-ordinates, which are also the master nodes for the design elements.

k) **Subroutine OUTPUT:** The stresses and displacements from each iteration are stored by this subroutine. Final stresses are utilised for tabulating data, plotting graphs, etc.

3.6 Steps involved in the computation

The steps taken up sequentially by GSO are presented in the flowchart shown in Figure 3.9.

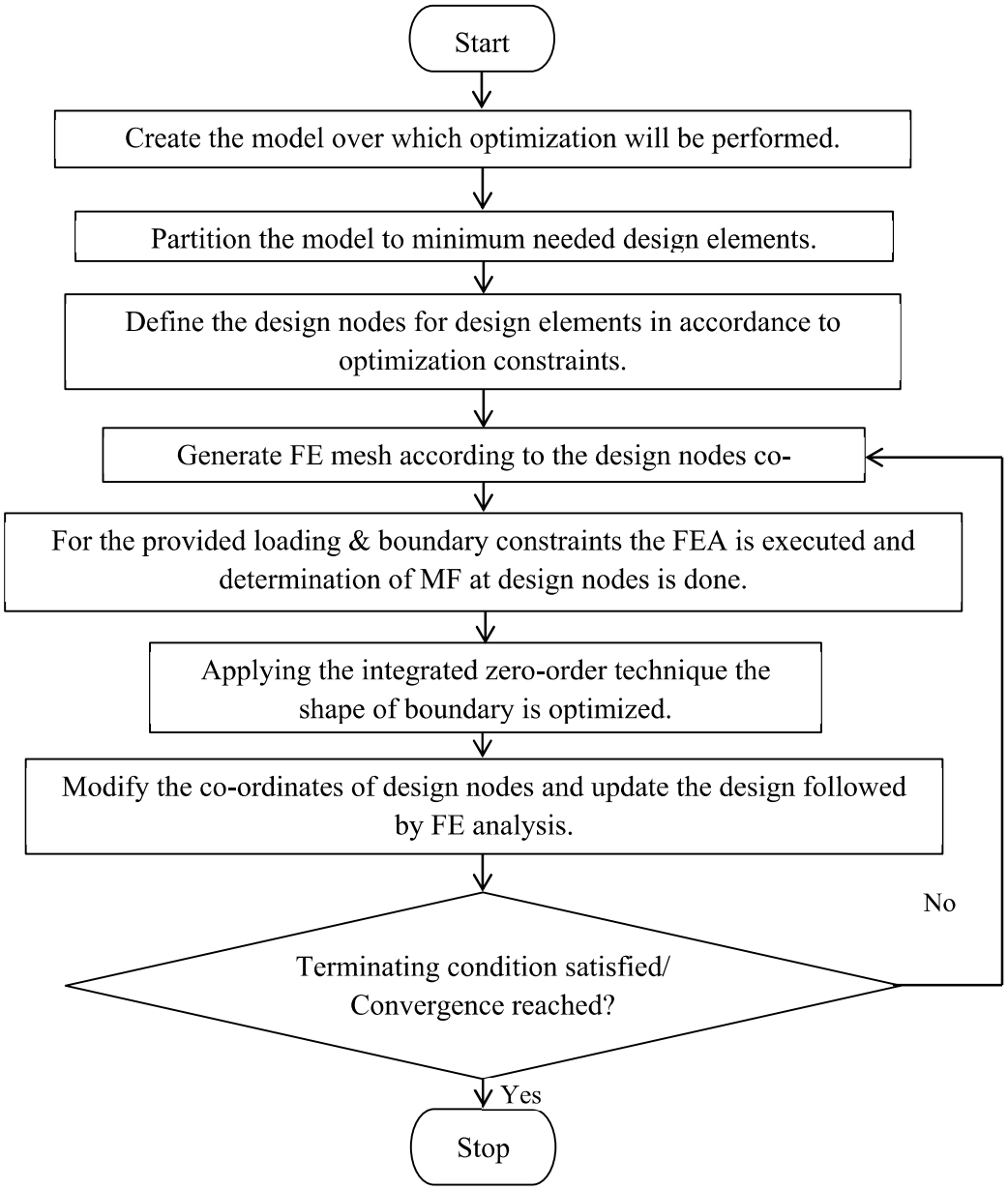

Figure 3.9: Working flowchart of GSO.

3.7 Numerical Illustrations

Using GSO, a few examples of shape optimization of precast structural members have been carried out. Different types of beams and plates have been considered with varying loading and support conditions over it and have been analyzed for shape optimization. The dimension of the beam considered here is length, width, and thickness as 300 mm, 50 mm, and 40 mm respectively, and for the plate, it is 60 mm radius with 2 mm thickness and a square hole of 20 mm sides at the centre of the plate. Four design elements have been considered in both beam and plate with a total of 18 design nodes. The structural element is then discretised into 48, nine-noded Lagrangian plane stress elements forming a total of 231 nodes. The discretization of the beam and plate in finite elements with the position of master nodes is shown in Figure 3.10. Young's modulus and Poisson's ratio for a single material beam and plate are taken as $2x10^5$ N/mm^2 and 0.3 respectively. Examples of structures with initial imperfection and composite material have also been considered and tested. The results of these are categorised into four cases.

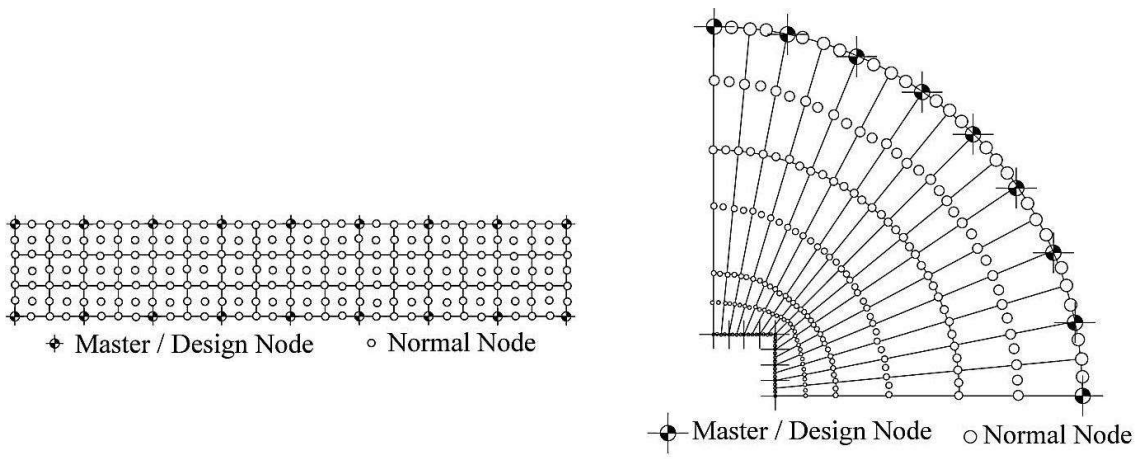

(a) (b)

Figure 3.10: Discretization structural element in 48 nine noded Lagrangian plane stress element (a) Beam (b) Plate

3.7.1 Case-1: Structures with perfect boundaries and single material

GSO optimization is carried out on different beams and plates, consisting of a homogeneous material and possessing a consistent cross-sectional profile, subjected to different loading and support conditions.

3.7.1.1 Fixed-beam

The beam here is given fixed support. All eighteen design nodes present on the boundary of the beam have been taken into consideration for shape optimization. The optimized shape of the beam for loading with a 20,000 N load concentrated at the centre of the span, two 10,000 N loads concentrated at a distance of one-third from each end of the span, and a 20,000 N load uniformly distributed along the span have been obtained. σ_t in each case is taken as 30 N/mm^2. The software took 112, 186, and 249 iterations respectively to get the optimized shape. The optimized shapes obtained due to different loadings are shown in Figure 3.11 and the 'σ' distribution for the initial and optimized shape is shown in Figure 3.12.

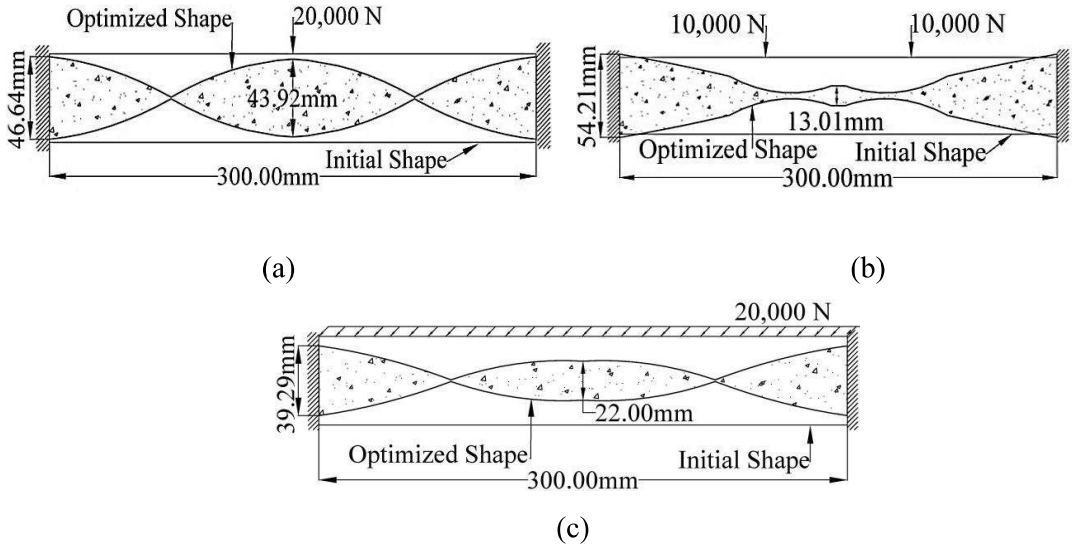

Figure 3.11: Optimized Shape of fixed beam with (a) Point load (b) Two point loads (c) Uniformly distributed load.

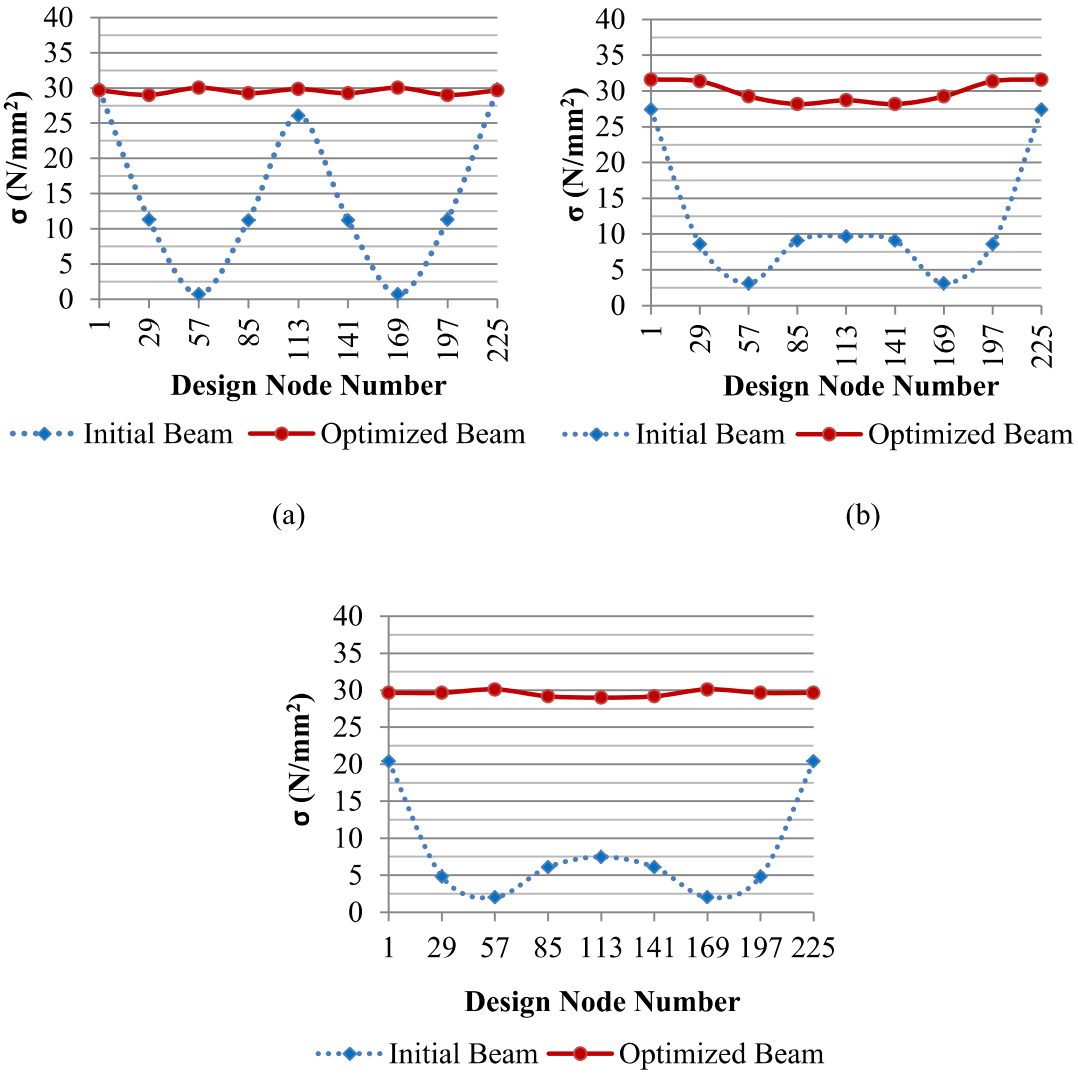

Figure 3.12: Maximum shear stress distribution in fixed beam with (a) Point load (b) Two point loads (c) Uniformly distributed load.

3.7.1.2 Cantilever beam

The beam is now made cantilever and all eighteen design nodes present on the boundary of the beam have been taken into consideration for shape optimization. The optimized

shape of the beam for loading with a 10,000 N load concentrated at the free end of the span, two 5,000 N loads concentrated at a distance of 150 mm and 300 mm respectively from the fixed end of the beam and 10,000 N load uniformly distributed along the span have been obtained. σ_t in each case is taken as 30 N/mm^2. The software took 86, 92, and 118 iterations respectively to get the optimized shape. The optimized shapes obtained due to different loadings are shown in Figure 3.13 and the 'σ' distribution for the initial and optimized shape is shown in Figure 3.14.

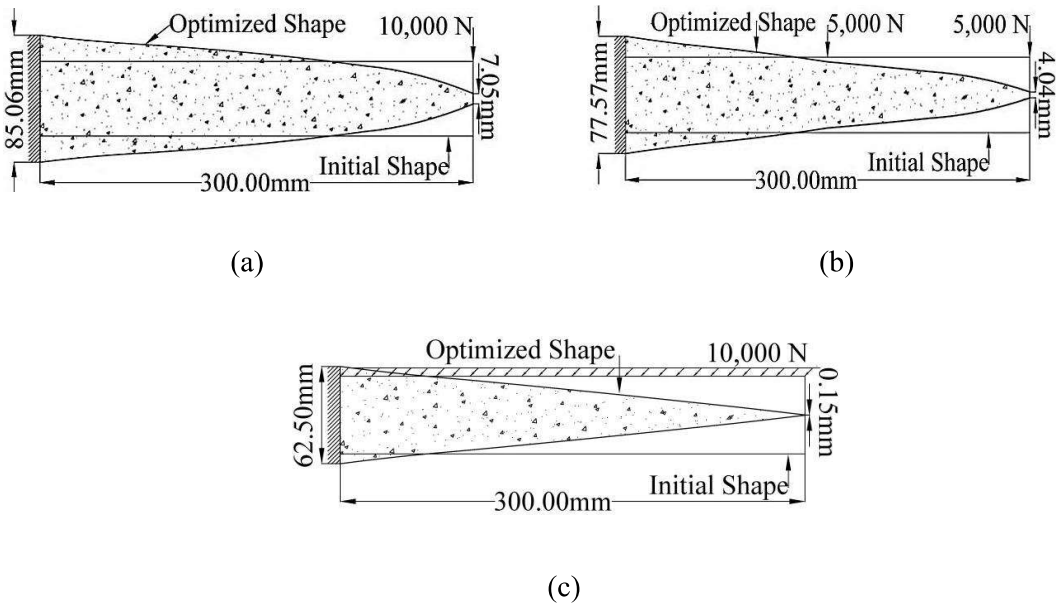

Figure 3.13: Optimized Shape of a cantilever beam with (a) Point load (b) Two point loads (c) Uniformly distributed load.

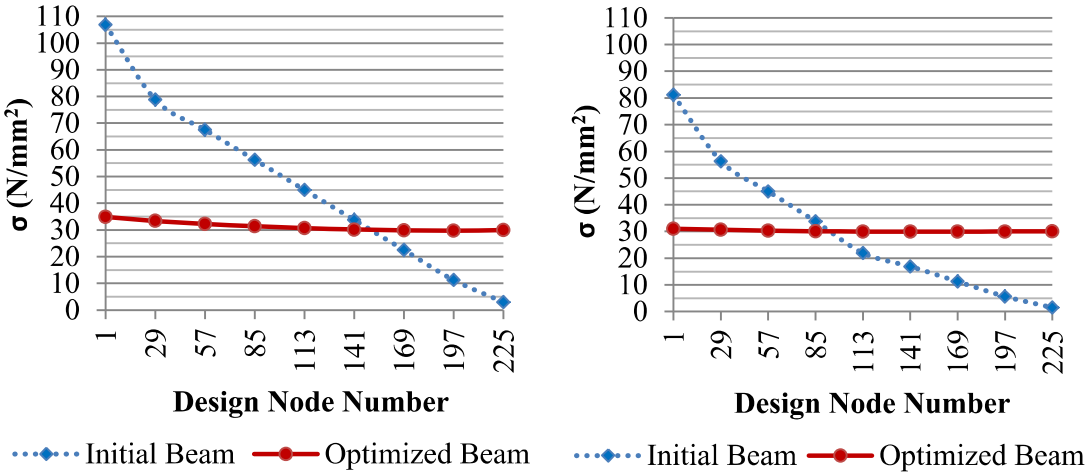

(a)

(b)

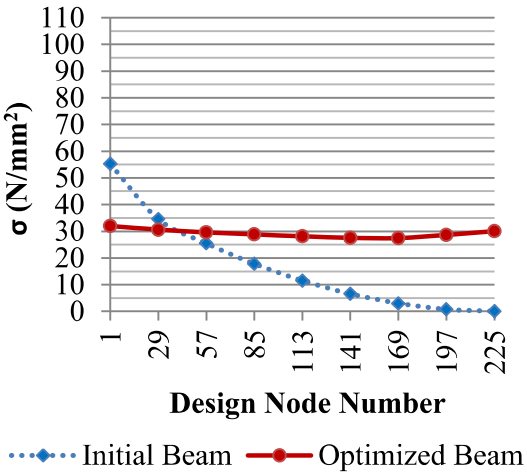

(c)

Figure 3.14: Maximum shear stress distribution in a cantilever beam with (a) Point load (b) Two point loads (c) Uniformly distributed load.

3.7.1.3 Simply supported Beam

For a simply supported beam, all eighteen design nodes present on the boundary of the beam have been taken into consideration for shape optimization. The optimized shape of the beam for loading with a 20,000 N load concentrated at the centre of the span, two 10,000 N loads concentrated at a distance of one-third from each end of the span, and a 20,000 N load uniformly distributed along the span have been obtained. σ_t in each case is taken as 30 N/mm^2. The software took 25, 27, and 33 iterations respectively to get the optimized shape. The optimized shapes obtained due to different loadings are shown in Figure 3.15 and the 'σ' distribution for the initial and optimized shape is shown in Figure 3.16.

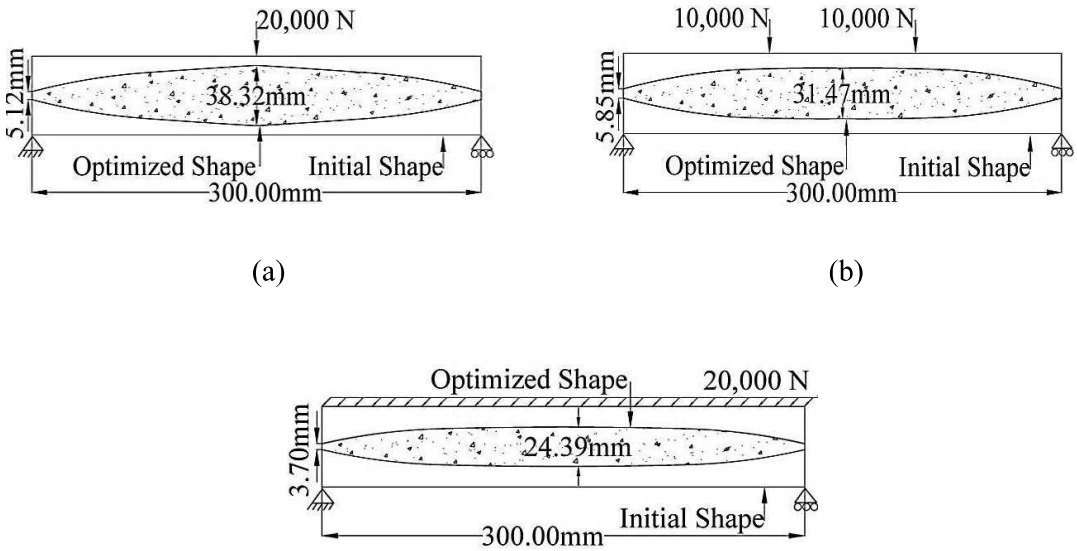

Figure 3.15: Optimized Shape of the simply supported beam with (a) Point load (b) Two point loads (c) Uniformly distributed load.

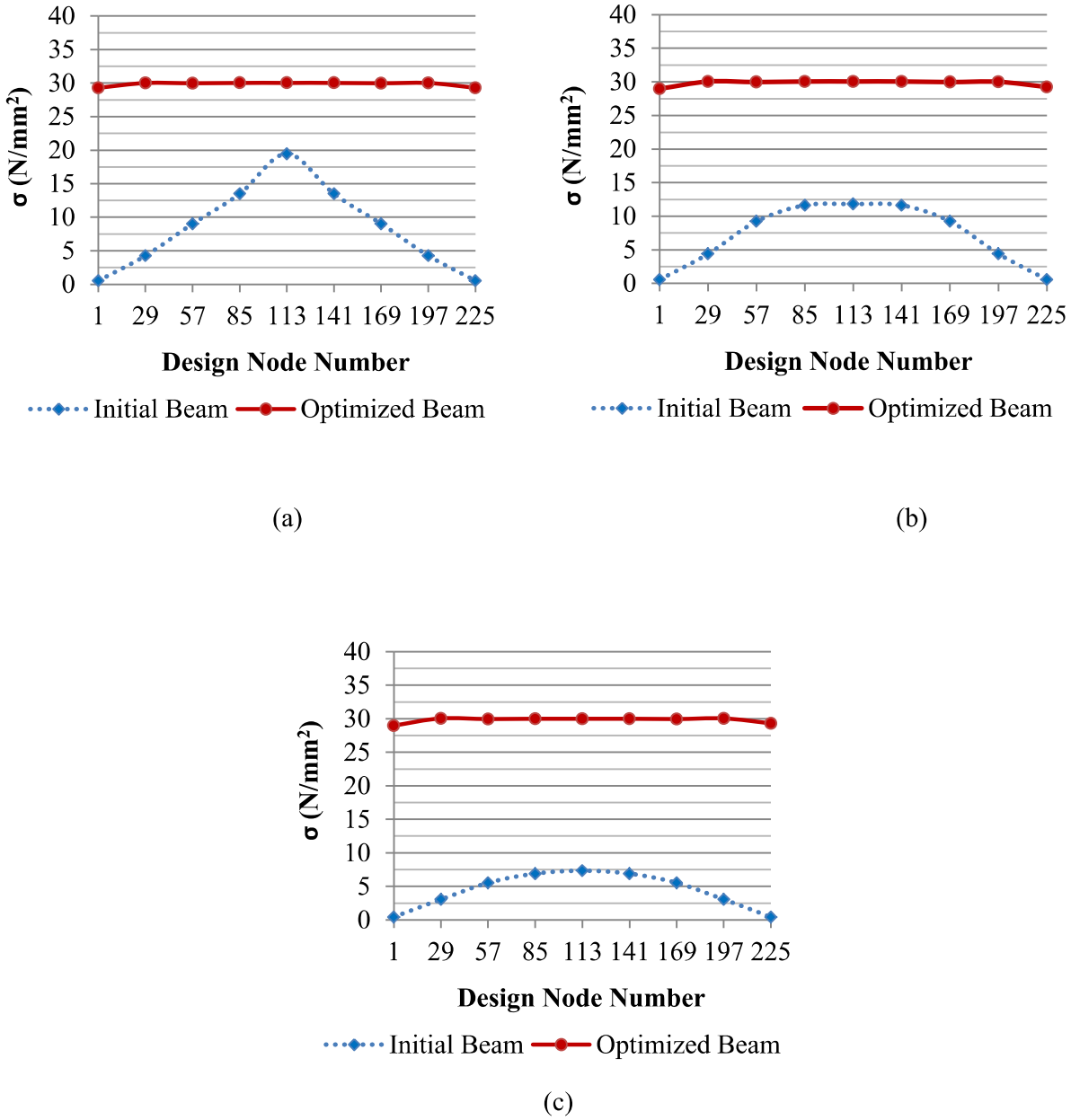

Figure 3.16: Maximum shear stress distribution in simply supported beam with (a) Point load (b) Two point loads (c) Uniformly distributed load.

3.7.1.4 Circular plate with a square hole

While optimizing a circular plate with a square hole, due to the symmetry of the circular plate, only a quarter part is being considered and analyzed for shape optimization. The

design nodes are taken on the inner edge only as the stress concentration is high over there and optimization is to be done from the inner edge. Nine inner edge design nodes are considered. The optimized shape of the plate with a square hole for 2,000 N load concentrated at the centre of the quarter circumference as shown in Figure 3.16(a), two 1,000 N load concentrated as shown in Figure 3.16(b) and 2,000 N load uniformly distributed along the quarter circumference of the plate as shown in Figure 3.16(c) have been obtained. σ_t in each case is taken as 15 N/mm^2. The software took 51, 50, and 51 iterations respectively to get the optimized shape. The optimized shapes obtained due to different loadings are shown in Figure 3.17 and the 'σ' distribution for the initial and optimized shape is shown in Figure 3.18.

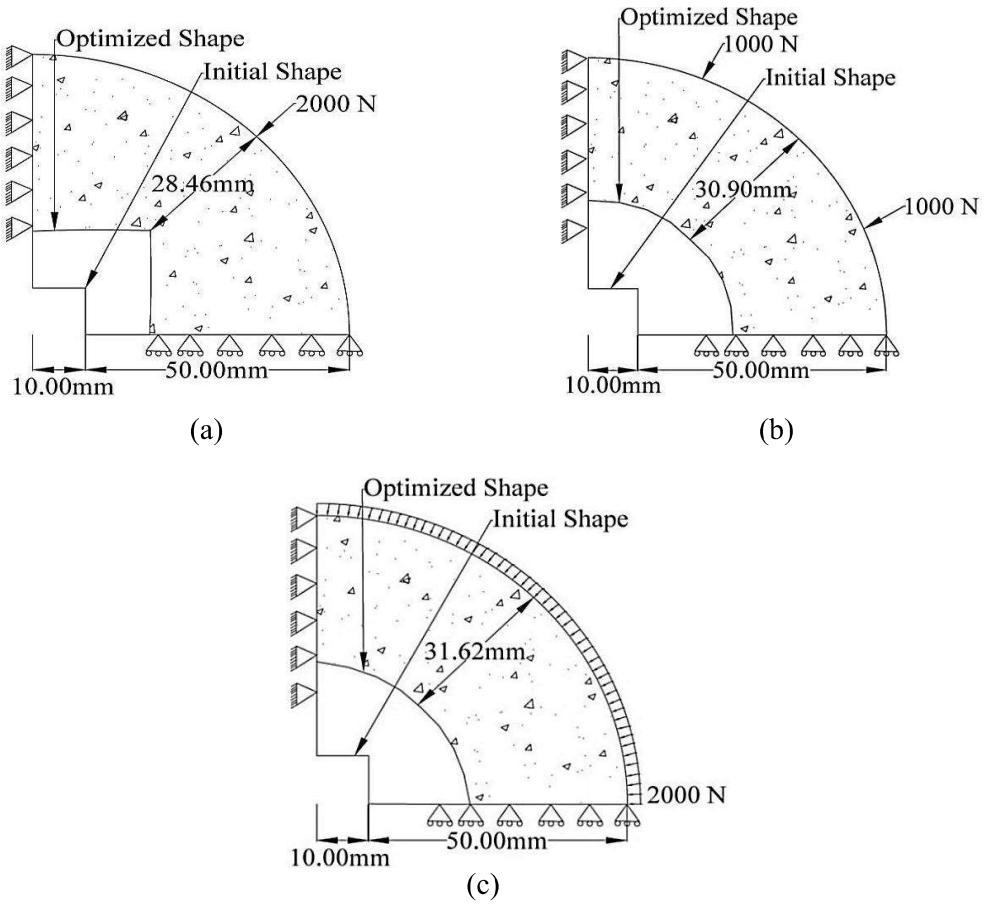

Figure 3.17: Optimized shape of a circular plate with a square hole with (a) Point load (b) Two point loads (c) Uniformly distributed load.

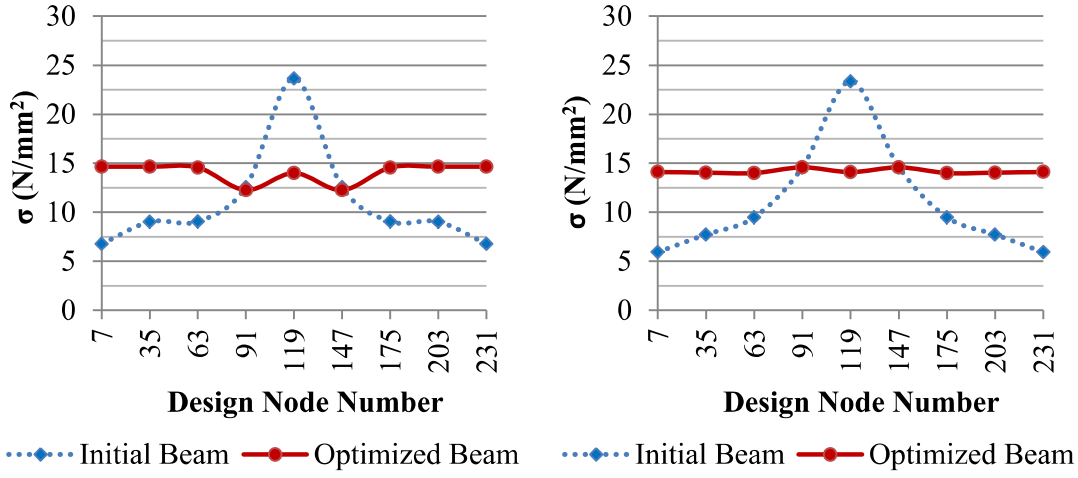

(a) (b)

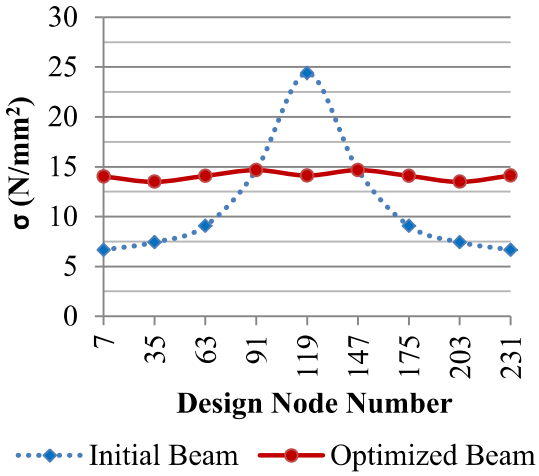

(c)

Figure 3.18: Maximum shear stress distribution in a circular plate with a square hole with (a) Point load (b) Two point loads (c) Uniformly distributed load.

3.7.2 Case-2: Effect of initial imperfection on shape optimization

It is not always possible to design a perfectly shaped structure. Hence there might be chances that initial imperfection is induced due to human error while designing the structure. In that case, the software should be able to recognise the initial imperfection

and perform the shape optimization accordingly to get the best results. For this purpose, a few examples are presented with given initial imperfections.

3.7.2.1 Fixed-beam with initial imperfection

The beam considered in section 3.7.1.1 is in the first case, given a gradual imperfection of ±4 mm at the mid of the span and in the second case, a gradual imperfection of ±4 mm at the middle third distance from both ends of the span and optimized for a point load. σ_t is taken as 30 N/mm^2. The software took 164 and 145 iterations respectively to get the optimized shape. The optimized shapes of the beam and 'σ' distribution are presented in Figure 3.19 and Figure 3.20 respectively.

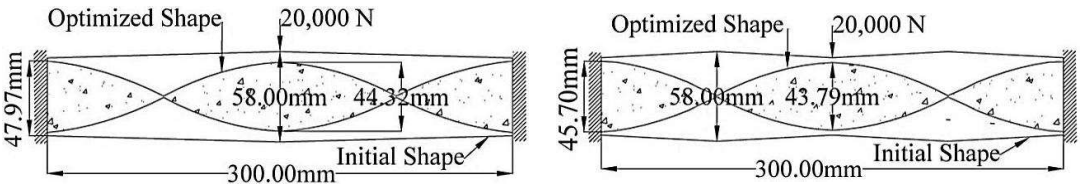

(a) (b)

Figure 3.19: Fixed beam with initial imperfection: (a) ±4 mm imperfection at mid-span, (b) ±4 mm imperfection at a middle third distance from both ends of the span

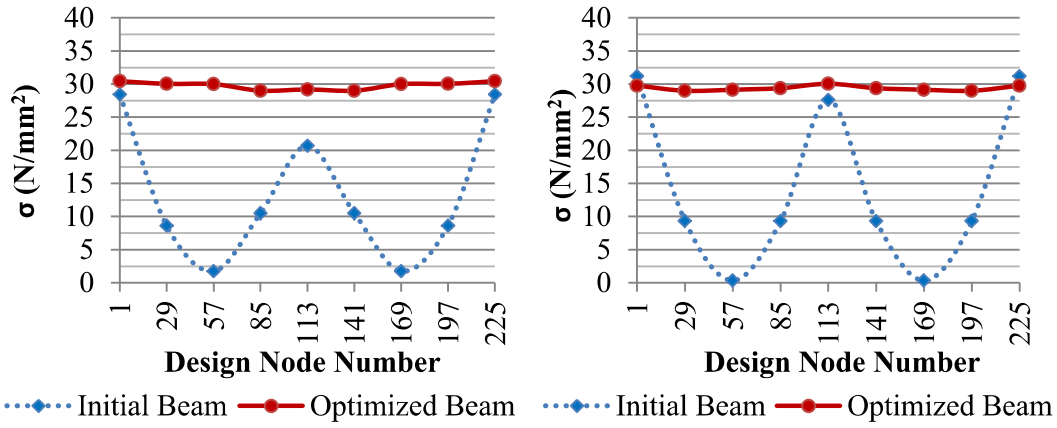

Figure 3.20: Maximum shear stress distribution in fixed beam with initial imperfection: (a) ±4 mm imperfection at mid-span, (b) ±4 mm imperfection at a middle third distance from both ends of the span

3.7.2.2 Cantilever beam with initial imperfection

The beam considered in section 3.7.1.2 in the first case is given the initial gradual imperfection with a maximum of ±1 mm at the middle third point from both ends of the span and in the second case initial imperfection was then increased to ±5 mm and the shape optimization was done. σ_t is taken as 30 N/mm^2. The software took 85 and 82 iterations respectively to get the optimized shape. The optimized shape of the beam and the 'σ' distribution is presented in Figure 3.21 and Figure 3.22 respectively.

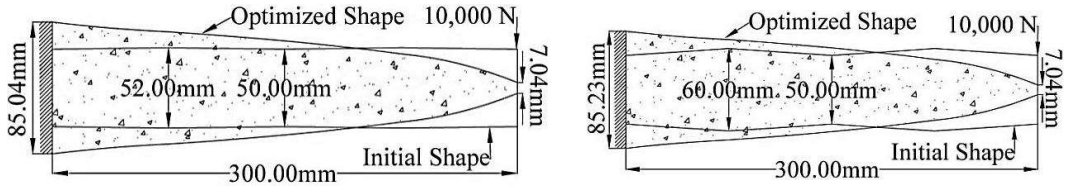

(a) (b)

Figure 3.21: Cantilever beam with initial imperfection: (a) ± 1mm imperfection at both ends of the middle third part, (b) ± 5mm imperfection at both ends of the middle third part

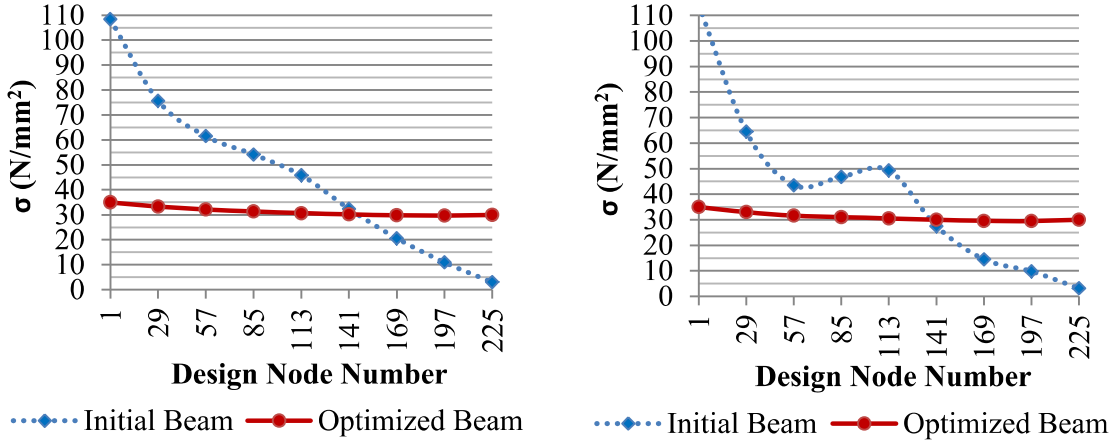

(a) (b)

Figure 3.22: Maximum shear stress distribution in a cantilever beam with initial imperfection: (a) ± 1mm imperfection at both ends of the middle third part, (b) ± 5mm imperfection at both ends of the middle third part

It can be seen that the final optimized shape remains the same as obtained in sections 3.7.1.1 and 3.7.2.1. for point load. However the stress distribution on beams before optimization changes, which is picked up effectively by the software and can be seen from the graphs. Hence for beams of similar material specifications, dimensions,

loading and support conditions the optimized shape obtained is the same irrespective of initial imperfections.

3.7.2.3 Circular plate with a square hole with imperfection

In the plate considered in section 3.7.1.4 in the first case, initial gradual imperfection on the square cut-out has been given as +1 mm on the sides and +2mm at the corner and in the second case, an uneven initial imperfection of +3 mm on one side and +2 mm on other side and +5 mm on the corners has been given. σ_t is taken as 15 N/mm^2. The software took 48 and 41 iterations respectively to get the optimized shape. The optimized shape and 'σ' distribution have been presented in Figure 3.23 and Figure 3.24 respectively.

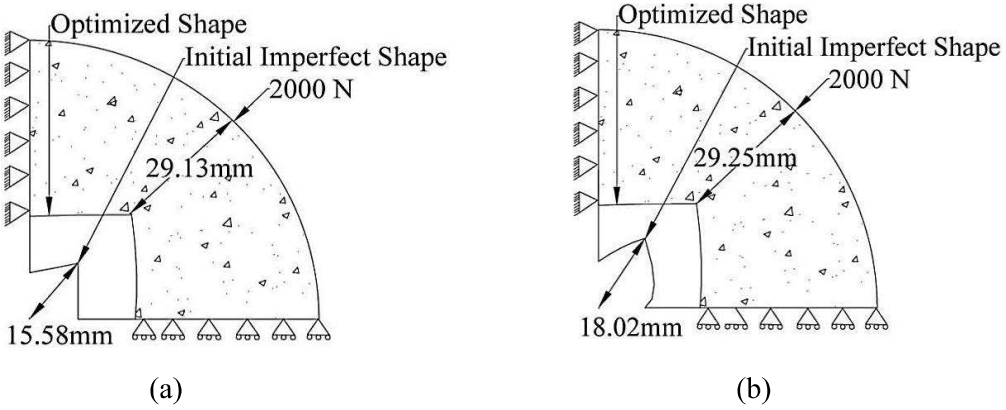

(a) (b)

Figure 3.23: Circular plate with a square hole with imperfection: (a) $\pm$ 2 imperfection at the corner of the hole, (b) $\pm$ 5 imperfection at the corner of the hole

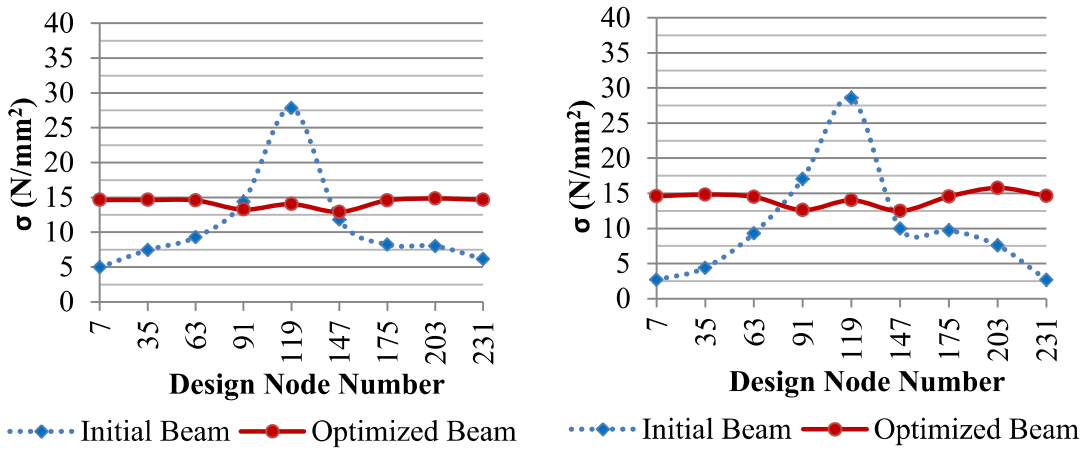

Figure 3.24: Maximum shear stress distribution in the circular plate with a square hole with imperfection: (a) ± 2 imperfection at the corner of the hole, (b) ± 5 imperfection at the corner of the hole

Similar results, as obtained in imperfect beams are also obtained with a circular plate with a hole. It can be deduced that software is fully capable of understanding the initial imperfection or intricacies which might creep in due to human error and act in accordance with that, so as to give an error-free and correct optimized shape for the structures.

3.7.3 Case-3: Beams with flat tops

In-case, if flat tops due to functional reasons are needed in the beam, they can also be given with properly optimized shape using this software. In such a case only the lower nodes are assigned as design nodes. Examples of such cases are given in sections 3.7.3.1, 3.7.3.2 and 3.7.3.3:

3.7.3.1 Flat top fixed beam

The beam considered in section 3.7.1.1 is now optimized in a way that the top surface remains flat. Here only the lower nodes have been considered as design nodes so that the change in shape for optimization occurs from the lower part of the beam keeping the upper part flat. The optimized shape of the beam for loading with a 20,000 N load concentrated at the centre of the span, two 10,000 N loads concentrated at a distance of one-third of the length from each end of the span, and a 20,000 N load uniformly distributed along the span have been obtained. σ_t in each case is taken as 30 N/mm^2. The software took 209, 294, and 264 iterations respectively to get the optimized shape. The optimized shapes with top surface flat obtained due to different loadings are shown in Figure 3.25 and the 'σ' distribution for the initial and optimized shape is shown in Figure 3.26.

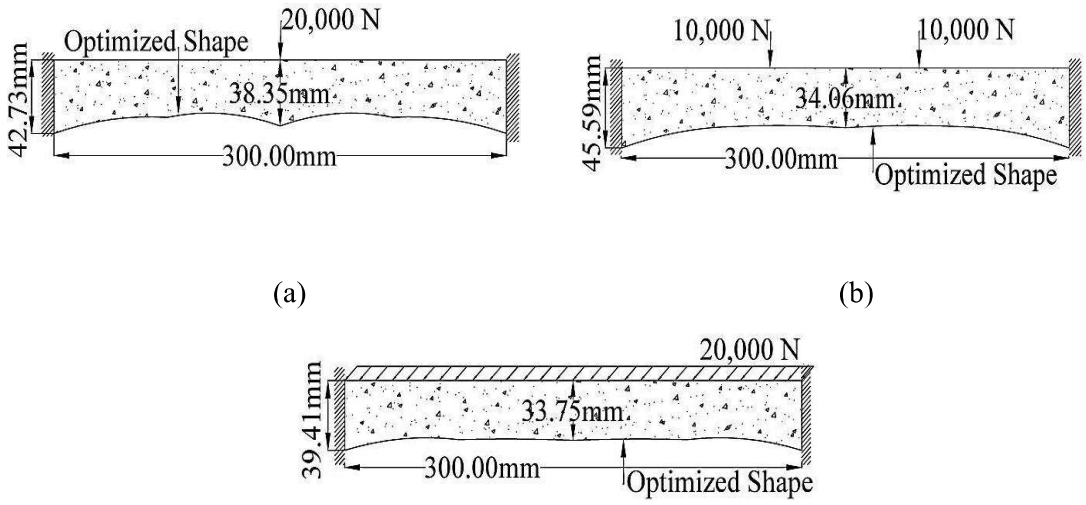

Figure 3.25: Optimized Shape of the flat top fixed beam with (a) Point load (b) Two-point loads (c) Uniformly distributed load.

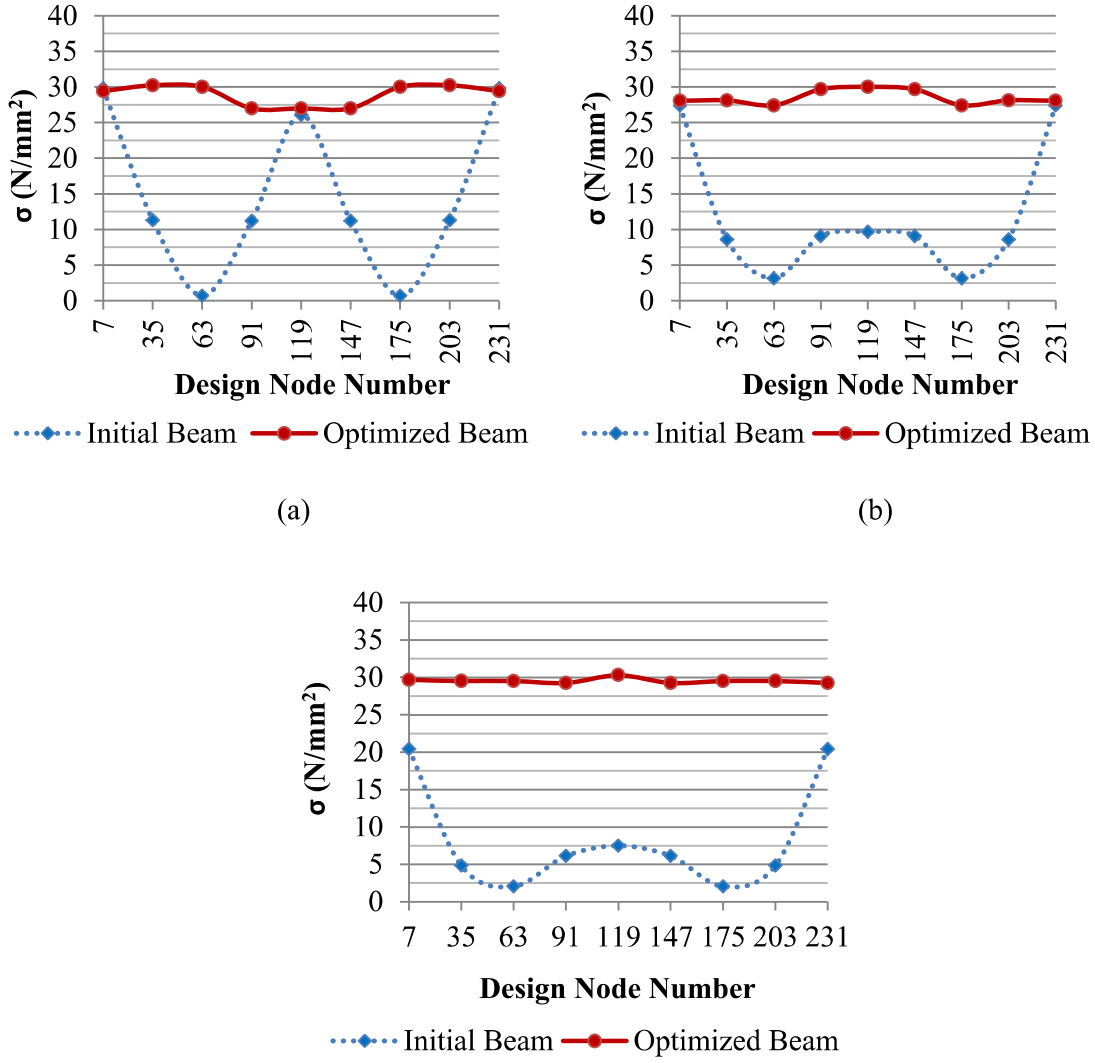

Figure 3.26: Maximum shear stress distribution in flat top fixed beam with (a) Point load (b) Two point loads (c) Uniformly distributed load.

3.7.3.2 Flat top cantilever beam

The cantilever beam considered in section 3.7.1.2 is taken. Nine design nodes have been taken on the bottom face of the beam. The optimized shape of the cantilever beam with a flat top for loading with 10,000 N load concentrated at the free end of the span, two 5,000 N loads concentrated at a distance of 150mm and 300mm respectively from the

fixed end of the beam and 10,000 N load uniformly distributed along the span have been obtained. σ_t in each case is taken as 30 N/mm^2. The software took 171, 193, and 234 iterations respectively to get the optimized shape. The optimized shapes obtained due to different loadings are shown in Figure 3.27 and the 'σ' distribution for the initial and optimized shape is shown in Figure 3.28.

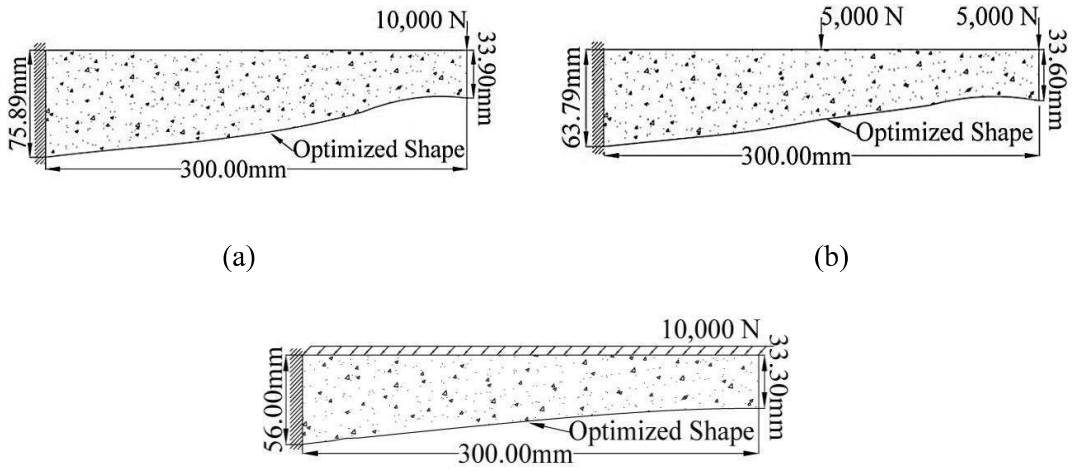

Figure 3.27: Optimized Shape of a flat top cantilever beam with (a) Point load (b) Two point loads (c) Uniformly distributed load.

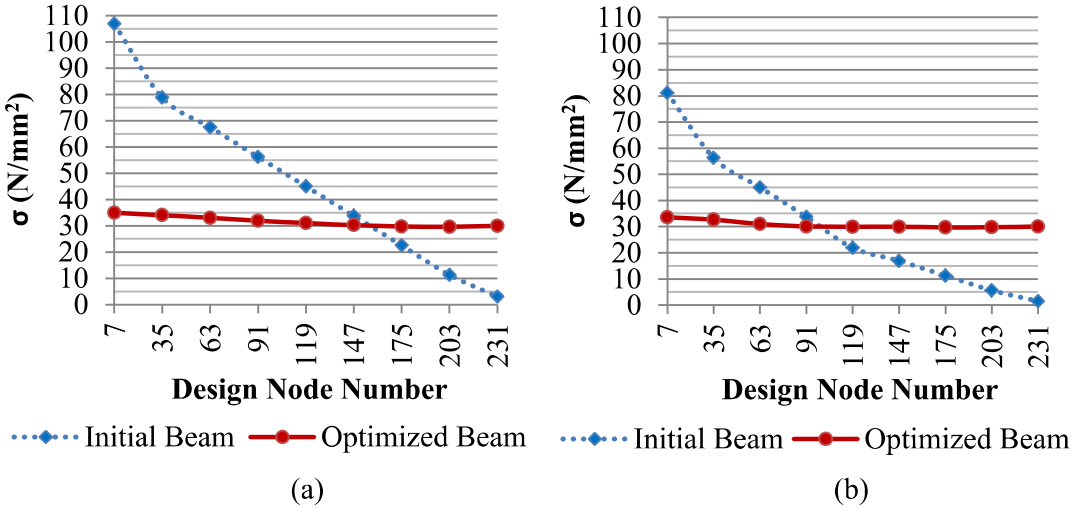

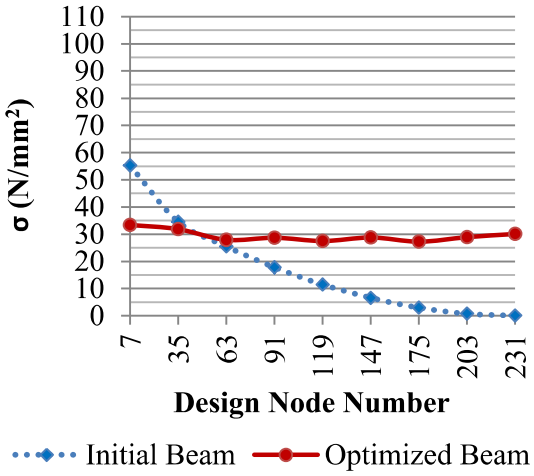

(c)

Figure 3.28: Maximum shear stress distribution in a flat top cantilever beam with (a) Point load (b) Two point loads (c) Uniformly distributed load.

3.7.3.3 Flat top simply supported beam

The simply supported beam considered in section 3.7.1.3 is taken and optimized to get a flat top surface. Here nine design nodes present on the bottom face of the beam have been taken into consideration for shape optimization. The optimized shape of the beam for loading with a 20,000 N load concentrated at the centre of the span, two 10,000 N loads concentrated at a distance of one-third from each end of the span, and a 20,000 N load uniformly distributed along the span have been obtained. σ_t in each case is taken as 30 N/mm^2. The software took 36, 39, and 37 iterations respectively to get the optimized shape. The optimized shapes obtained due to different loadings are shown in Figure 3.29 and the 'σ' distribution for the initial and optimized shape is shown in Figure 3.30.

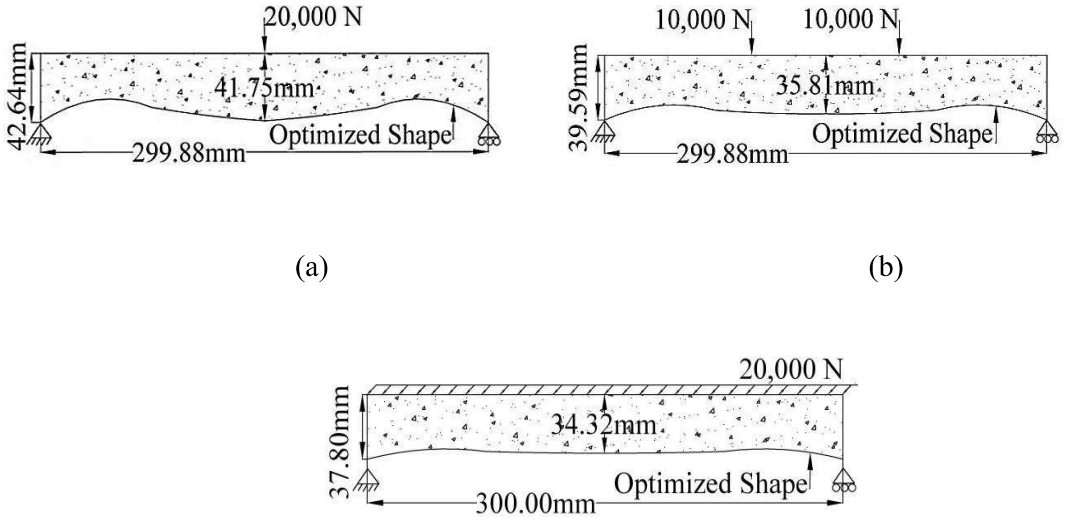

Figure 3.29: Optimized Shape of flat top simply supported beam with (a) Point load (b) Two point loads (c) Uniformly distributed load.

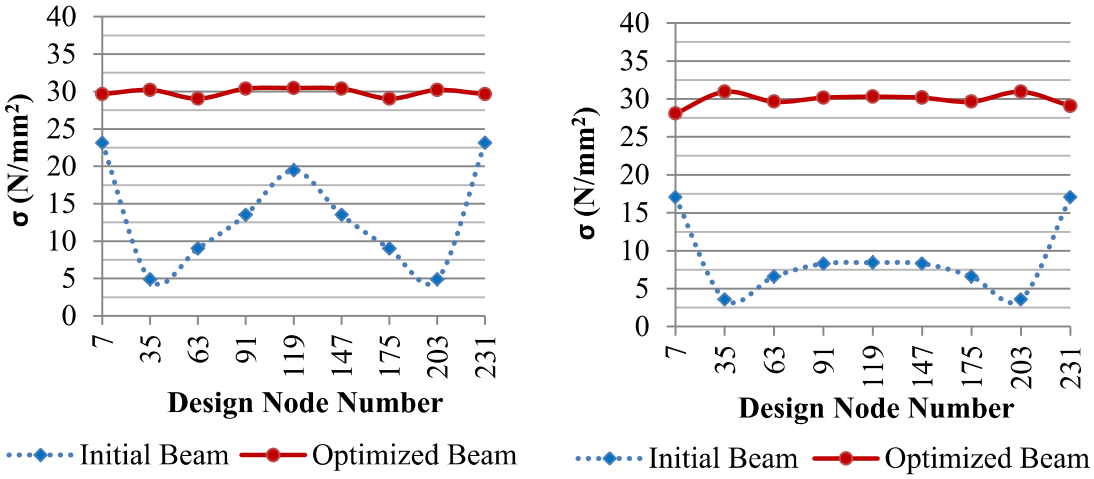

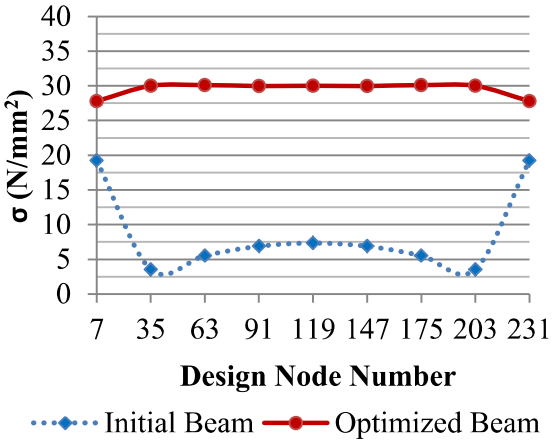

(c)

Figure 3.30: Maximum shear stress distribution in flat top simply supported beam with (a) Point load (b) Two point loads (c) Uniformly distributed load.

The difference in the final optimized shape in the case of a flat top and without flat-top beams can be seen here.

3.7.4 Case-4: Composite fixed beams

The use of composite beams has increased a lot in civil engineering applications nowadays due to various added advantages. Hence it is necessary to analyze the optimized shape for composite beams also. In this illustration, for variation, a fixed beam different in dimension than what is considered in section 3.7.1.1 and consisting of two materials has been considered. The length, width, and thickness are taken as 240 mm, 40 mm and 10 mm respectively. At the location at which the bending moment reaches zero, the different materials are employed and changed. Here in this illustration, the bending moment is becoming zero at two points, which are 60 mm right of the left support and 60 mm left of the right support. The material in between i.e. from 60 mm to

180 mm of the left support of the beam is kept consistent with Young's modulus of $2x10^5$ N/mm^2. From 0 mm to 60 mm and from 180 mm to 240 mm of left support a second material has been used. The second material's Young's modulus is systematically altered as $2x10^4$ N/mm^2 (M-1), $5x10^4$ N/mm^2 (M-2), $10x10^4$ N/mm^2 (M-3), $15x10^4$ N/mm^2 (M-4), $2x10^5$ N/mm^2 (M-5) to get an idea of change in co-ordinates of the optimized shape obtained by varying the property of the material. Four design elements have been considered with a total of 18 design nodes. It is discretised in forty-eight, Lagrangian plane stress elements with 9 nodes each forming a total of 231 nodes. Due to symmetry in loading and geometrical condition, only nine design nodes present on the top face of the beam have been taken into consideration for shape optimization. σt is taken as 60 N/mm2. The number of iterations taken in order to achieve the optimal shape is 106 for M-1, 119 for M-2, 165 for M-3, 170 for M-4, and 175 for M-5. The optimized shape and change in shape co-ordinates due to change in materials are presented in Figure 3.31. 'σ' distribution for the initial and optimized shape is shown in Figure 3.32.

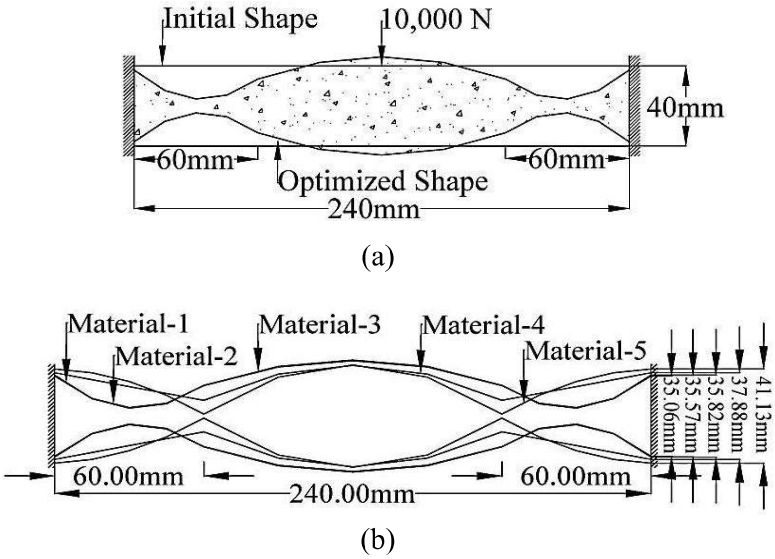

Figure 3.31: (a) Composite fixed beams, (b) Different optimized shapes with the change in material

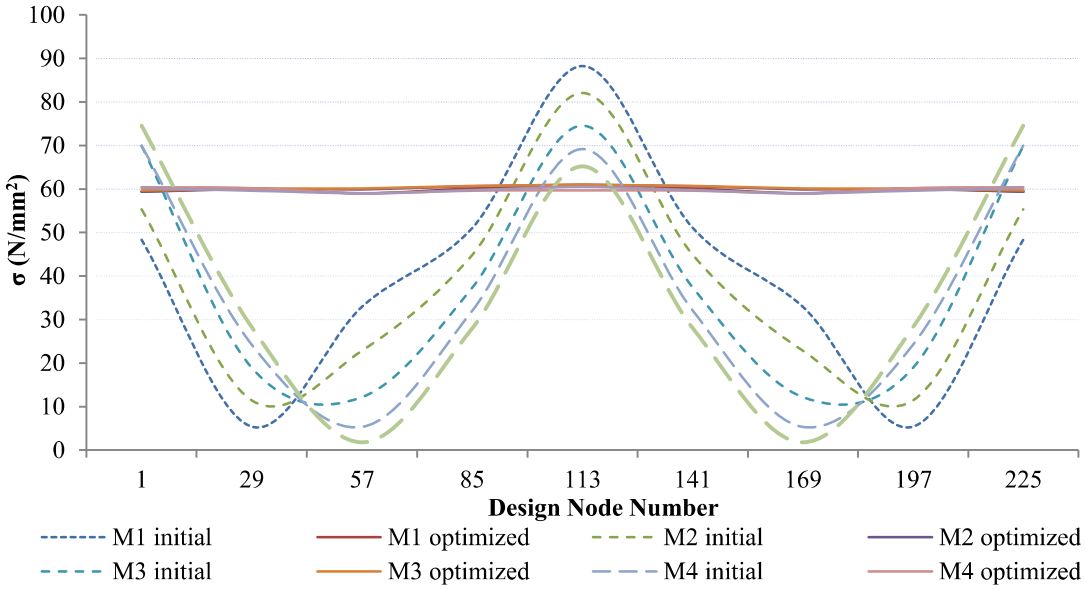

Figure 3.32: Maximum shear stress distribution in composite fixed beams: M-1, M-2, M-3, M-4 and M-5.

3.8 Discussion of the results

The results obtained using the above-shown examples give an idea about the effectiveness of GSO software for the purpose of shape optimization. In Case-1 different types of beams are considered and it is seen that the number of iterations to reach the convergence for the final optimized shape increases with an increase in the complexity of the loading pattern. In Case-2 it is seen that even after induction of some initial imperfection due to humanly possible errors of different magnitude, for the same structure, the final optimized shape remains the same. This shows that the shape is optimized until the fully stressed criterion is reached irrespective of the initial conditions being imperfect. However, with certain initial imperfections the number of iterations to reach convergence changes. In Case-3 optimized shapes of structures with the flat top have been obtained. Since the design nodes on the lower bottom are only

taken it takes more iterations to reach convergence than what is taken by non-flat top cases. In Case-4 it is seen that with the change in materials, the co-ordinates for optimized shape changes and the number of iterations are also different in each case. This indicates that the software is responsive to the changes given in material properties. In each case, however, a properly optimized shape with maximum shear stress within the target limit at each design node is obtained. The number of iterations needed to reach the convergence can be reduced by increasing the length of nodal movement from 0.25 length to full length but doing this will decrease the accuracy of results obtained.

3.9 Concluding Remarks

This chapter of the thesis successfully discusses an integrated zero-order method also termed an integrated gradientless method for shape optimization of structures. This has been embodied in a FORTRAN code as a software labelled GSO. The criteria of fully stressed design have been effectively used and satisfied to obtain the optimized shape for structures. The value of (σ) obtained is very much near to the (σ_t) taken. The use of minimal design elements and proper design nodes has resulted in faster convergence without compromising the quality of results. The capabilities of the GSO have been effectively demonstrated by a few examples like initial imperfection, composite beams, and flat tops with different sets of initial conditions and the results of which are demonstrated in the figures. The proposed approach is found to carry out successful shape optimization for different structures with varying geometrical and material parameters.